Synthesis, Characterization of Silver Doped Hydroxyapatite Nanoparticles for Biomedical Applications

Sneha S Bandgar[1,2], Tanaji V Kolekar[3], Shailesh S Shirguppikar[3], Mahesh A Shinde[3], Rajendra V Shejawal[1*], Sambhaji R Bamane[2*]

[1]Department of Chemistry, Lal Bahadur Shastri College, Satara, 415002, M.S., India

[2]Department of Chemistry, R.S.B.Mahavidyalaya, Aundh, Satara, 415002, M.S., India

[3]Rajarambapu Institute of Technology, Islampur, Sangli 415 414, M.S., India

ABSTRACT

Calcium based Bio ceramics are potentially attractive a wide range of medical applications. The effect of Silver substitution on the biocompatibility of hydroxyapatite (HA) under the physiochemical conditions has been investigated. Various samples of Silver doped hydroxyapatite (Ag-HA) with different concentration (0, 0.5, 1.0, 1.5, 2.0, 2.5 mol%) were successfully synthesized by solution combustion method and characterized by X-ray diffraction (XRD), transmission electron microscopy (TEM), and scanning electron microscopy (SEM), and thermal analysis techniques. XRD and TEM results reveal uniform and crystalline Ag-HA nanoparticles.

Keywords: Solution combustion processes, Apatite composites, Antibacterial, Biomedical applications

INTRODUCTION

During recent years, there have been efforts in developing Nanocrystaline Calcium orthophosphate to enhance their biological and mechanical properties for use in biomedical applications. Calcium orthophosphate based inorganic bio ceramic materials have a wide range of biomedical applications [1]. Bioresorbable and Bioactive phases of calcium phosphate bioceramic materials are choice for bone-tissue engineering application because of their similar inorganic composition with the mineral phases of natural bone, excellent biocompatibility and osteoconductivity [2,3]. In 1920 it is reported the first successful medical application of calcium phosphate in humans [4]. Recently most widely-used bioresorbable and bioactive ceramics include calcium orthophosphates (CaP). They are present in bones, teeth and the tendons of mammals, giving these organs hardness and stability. They are known as non-ion-substituted calcium orthophosphates with a Ca/P molar ratio between 0.5 and 2.0. The most widely used member of the family of CaPs is hydroxyapatite (HA) [5]. Among different forms of calcium phosphate, hydroxyapatite (HA) is one of the most promising inorganic biomaterials. HA is the principal mineral constituents of natural bones and teeth [6].

Hydroxyapatite (HA) has been widely used as a biomaterial in orthopedics, bioengineering and dentistry, because of its good biocompatibility [7]. Synthetic Hydroxyapatite (HA) is the most promising because of good cation exchange rate with metals, excellent biocompatibility and high affinity for the pathogenic microorganisms [8-10]. It is reported that around 70-80% of implants are made of biocompatible metals [11]. With the introduction of a transient metal ion such as silver HA can be effective in controlling microorganisms Due to its ion-exchange capabilities [12].

Synthetic HA with metal doping for Biomedical applications has gained lot of attention because of the high flexibility and stability of apatite structure, a great number of cationic substitution are of potential application in the Biomedical field. There are many reports of the occupying of Ca sites by various divalent (Mg^{2+}, Sr^{2+}, Cd^{2+}, Ba^{2+}) and Trivalent cations (Al^{3+}, Fe^{3+}) [13]. However, now days the biggest current problem in the biomedical field is post-surgical infections arising from recent-implanted synthetic biomaterials, because these provide sites for potential bacterial adhesion [14]. However, there are some limitations of these bioceramic materials involving the possible release of harmful metal ions through wear and corrosion processes when they are exposed to aggressive body environment [15-17].

The metal release of toxic ions might cause adverse effects to the surrounding cells [18-20]. Silver has been known as a disinfectant for many years and has a broad spectrum of antimicrobial activity while exhibiting low toxicity towards mammalian cells. Various studies reported that the silver ions doped in the HA coatings play an important role in preventing or minimizing bacterial adhesion [21]. Furthermore, the reactivity of silver is high efficient when used in Nano sized particles due to their better contact with microorganisms [22]. higher concentration of Ag more than 300 ppb in human blood can cause side-effects in the form of leukopenia, Kidney and liver damage [23]. Therefore, optimization of Ag concentration in HA is critical to guarantee Ag/HA optimal antimicrobial ability without cytotoxicity [24].

Nano sized HA have been synthesized by many routes, including co-precipitation [25], sol-gel synthesis [26], emulsion methods [27], microwave precipitation [28] and mechano chemical methods [29]. Solution combustion synthesis (SCS) is invented in 1986, a large number of research efforts have been focused toward the preparation of important materials, mostly oxides, with improved properties [30]. In solution combustion synthesis, aqueous reactive solutions are used, where the precursors are mixed on the molecular level. The advantage of this process has been demonstrated by the use of different fuels and oxidizers, varying the oxidizer/fuel ratio and ignition sources, as well as combination of various synthesis approaches [31].

In the present investigation, Nano crystalline HA were prepared by a facile Solution combustion method. This work aims to study the effect of Ag on the Bioactivity of Nanocrystalline Hydroxyapatite (HA) under the physiological Conditions. Antibacterial effect was evaluated quantitatively against Gram-positive *Staphylococcus aureus* and Gram-negative *Escherichia coli*. The cytotoxicity assessments have been utilized to evaluated the bio-compability of nanocrystalline HA and Ag-HA with different concentration. Cytotoxicity of the prepared material has been studied by utilizing L929 (mouse Fibroblast) cell line for 12 and 24 h. For this trypan blue dye exclusion (TBDE) and MTT assays were performed to identify the possible toxicity of nanoparticles. The ultra-trace Ag doped HA nanocrystals may provide new opportunities in non-cytotoxic implant with antibacterial ability in bone tissue Engineering.

EXPERIMENTAL

Materials

Calcium nitrate tetrahydrate ($Ca(NO_3)_2 \cdot 4H_2O$), and *di*-Ammonium hydrogen orthophosphate ($(NH_4)_2HPO_4$) were purchased from Sigma-Aldrich and Silver nitrate ($AgNO_3$) were purchased from Thomas Baker. All chemicals used here were of analytical grade and used without further purification.

Synthesis of Ag-doped hydroxyapatite

Ag-doped hydroxyapatite (Ag-HA) with different concentration (0, 0.5, 1.0, 1.5, 2.0, 2.5 mol%) were prepared by modifying solution combustion method. For this, polyvinyl alcohol (PVA) was used as a fuel. In brief, the stoichiometric amounts of the nitrate precursors $Ca(NO_3)_2.4H_2O$, $AgNO_3$ and phosphate precursor $(NH_4)_2HPO_4$ were dissolved in double distilled water to form the solution of 0.1 M. The equimolar solution of PVA was prepared in double distilled water. The mixture of oxidants and fuel was placed onto a magnetic stirrer for 30 min. to get uniform mixing. Evaporation of water to form a gel of precursors was carried out at 100ºC and then the gel was heated at 300ºC to obtain a powder. The obtained powder of Ag-HA was then annealed at 950ºC for 6 h to remove carbon residues and then used for further analysis. The atomic ratio of (Ag+Ca)/P in the precursor were fixed at 1.67 in all of the cases. The dried mixture possesses the characteristics of combustion and can be ignited to start combustion reaction using muffle furnace. Various Ag-doped hydroxyapatite samples containing Ag content 0, 0.5, 1.0, 1.5, 2.0, 2.5 mol% were denoted as HA, Ag-HA-1, Ag-HA-2, Ag-HA-3, Ag-HA-4, Ag-HA-5, respectively.

Characterizations

Structural and morphological studies

The structural and morphological studies of the samples were studied using Thermo gravimetric analysis (TGA)**,** X-ray Diffractometer (XRD), Fourier Transform Infrared spectroscopy (FTIR), Scanning Electron Microscopy and Transmission Electron Microscopy (TEM) and. Phase identification and structural analysis of Ag-HA were studied using X-ray diffraction (Philip-3710) with Cu-Kα radiation in the 2θ range from 10ºC to 80ºC. The all patterns were analysed by X-pert high score plus software and compared with the Joint Committee on Powder Diffraction Standards (JCPDS) (JCDPS card No. 01-074-0565 and 01-074-1743). The surface morphology and particles sizes of the Ag-HA were determined by using transmission electron microscope (Philips CM 200 model) with an operating voltage of 20-200 kV and a resolution of 2.4 Å. The compositional analysis was done by energy dispersive spectroscopy (EDS, JEOL JSM 6360). A Perkin-Elmer spectrometer (Model No-783 USA) was used to obtain FTIR spectra of Al-HA samples in the range of 450-4000 cm^{-1} using KBr pellets.

Biocompatibility study

Antibacterial activity assay

The antibacterial ability of Nanocrystaline HA, Ag-HA-1, Ag-HA-2, Ag-HA-3, Ag-HA-4, Ag-HA-5 was carried out at 0.2, 0.4, 0.6, 0.8, 1.0 ppm by bacteriological plate counting methods using Gram negative *Escherichia coli* (*E. coli*, ATCC 8739) and Gram-positive *Staphylococcus aureus* (*S. aureus*, ATCC 6538). The bacterial strains were purchased from National Chemical laboratory, Pune. The bacteria were cultured in liquid nutrient broth medium at 35-37ºC for 12 h and adjusted to a concentration of about 10^7 CFU/mL. All used laboratory supplies below were sterilized in an autoclave at 121ºC for 20 min. Briefly, 0.5 g of each sterile Sample was dispersed in centrifugal tube containing *Buffered sodium chloride peptone (BECP)* (9 mL) and bacteria suspension (1 mL) and incubated at 30-35ºC for 4, 8, 12, 16, 32, 48 and 72 h. For subsequent bacteria counting, 100 µL of suspension was extracted from centrifugal tube and inoculated into solid nutrient agar medium followed by 24 h incubation at 35ºC. The bacterial colonies were counted. The antibacterial rates (R %) were calculated based on the formula which is already Reported elsewhere [32,33].

RESULTS AND DISCUSSION

Thermogravimetric analysis

TGA curve of pure HA and the representative Ag-HA-5 are shown in Figure 1. In TGA curve, five different stages were observed during the total weight loss. The first stage of weight loss is in between room temperature to 250ºC, which is due to the loss of physically adsorbed water. The second stage of weight loss is from 250 to 450ºC and this is due to loss of chemisorbed water, organic groups and solvent attached to the sample. The third stage is from 450 to 650ºC, The fourth stage is from 650 to 870ºC and the last fifth stage is from 870ºC the weight loss is less than 0.65%. Taking into consideration of TGA studies, all the samples are calcinated at 950ºC for their further characterization.
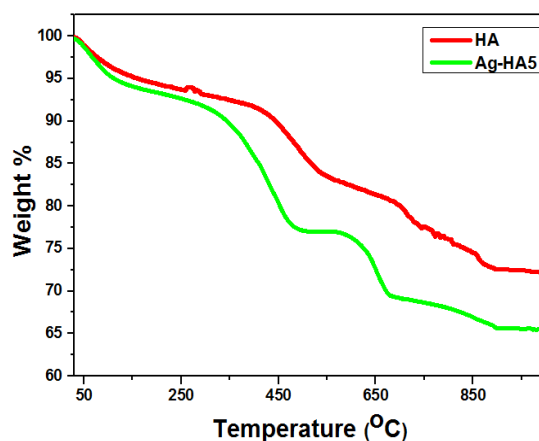

Figure 1: TGA pattern of pure HA and Ag-HA5 nanoparticles

XRD analysis

XRD patterns of the pure HA and Ag-HA samples are shown in Figure 2. The main phase in all samples was identified as hydroxyapatite (JCDPS No.01-074-0566) while the secondary phases of Ag (JCDPS No. 01-074-1743) were observed for doped samples with small percentage. HA showing space group P6₃/m with a hexagonal structure. It can be seen that, the lattice parameters of the prepared samples are in excellent agreement with standard data a=9.4240 Å, c=6.8790 Å and a=5.8500 Å, c=5.5000 Å for HA and Ag-HA, respectively. Gaussian fit of the most intense peak (211) was used to calculate the full width at half maxima for the determination of crystallite size (*D*) by using Scherrer equation:

$$D = \frac{0.9\lambda}{\beta \cos\theta} \qquad (2)$$

Where, *D* is the crystallite size, λ is the wavelength of Cu-Kα radiations (λ=1.5405 Å), θ is the corresponding Braggs diffraction angle and β is full width at half maxima of the most intense peak (211). The average crystallite sizes of HA and Ag-HA were found to be 28.50 nm and 22.12 nm, respectively. About pure HA similar result and phase purity were observed in our previous researcher [34]. The reflection peaks are quite broad, suggesting their Nanocrystallinity.
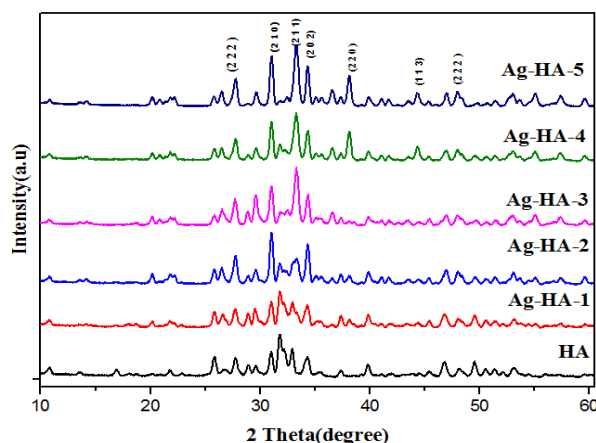

Figure 2: XRD patterns of pure HA and Ag-HA nanoparticles

80

SEM analysis

SEM technique was used to observe and analyse the agglomeration, microstructure and grain sizes of Ag-HA. SEM micrographs of HA and Ag-HA samples are depicted in Figure 3. SEM micrographs of samples are shown similar agglomerates that are consisting of fine crystallites and small size. It has been reported that crystal size distribution of bone plays an important role in bone fracture [35].
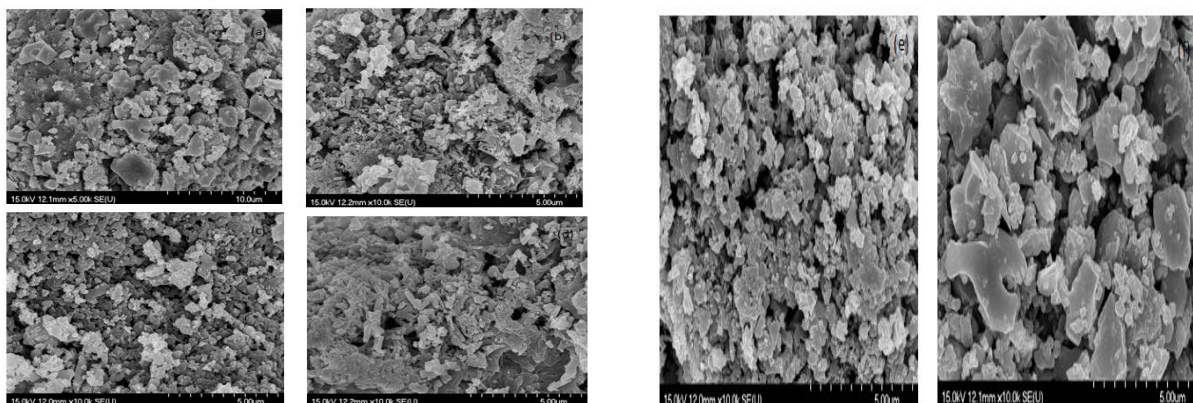

Figure 3: SEM images of (a) pure HA, (b) Ag-HA-1, (c) Ag-HA-2, (d) Ag-HA-3, (e) Ag-HA-4, and (f) Ag-HA-5

The EDS spectra was used for quantitative elemental analysis of the HA and Al-HA samples. Figure 4 shows EDS spectra of HA and a representative Al-HA sample. The EDS spectra indicate that samples are consistent with their elemental signals and stoichiometry is as expected. In the case of pure HA, the corresponding peaks are due to the presence of calcium (Ca), phosphor (P), and oxygen (O) while for Al-HA samples the observed peaks corresponds with aluminum (Al), calcium (Ca), phosphor (P), oxygen (O). This implies that the prepared samples are pure in nature. The elemental composition estimated from EDS analysis is tabulated in Table 1.

Table 1: The elemental composition estimated from EDS analysis

Sample	Atomic % composition			
	Ag	**Ca**	**P**	**O**
HA	-	32.33	19.52	48.15
Ag-HA-1	1.02	28.89	19.03	51.06
Ag-HA-2	1.51	28.13	18.97	51.40
Ag-HA-3	3.27	26.97	18.40	57.68
Ag-HA-4	4.48	23.12	15.93	58.29
Ag-HA-5	6.07	21.90	15.33	60.21

The Ca/P atomic ratios for pure Nanocrystalline HA are 1.66 which is in adjacent agreement with the standard Ca/P atomic ratio 1.67. The Ca/P atomic ratios (1.51, 1.48, 1.46.1.45, 1.42) for Ag-HA samples are little smaller than that of the standard. From Table 1, it is observed that there is a decrease in Ca/P atomic ratio in the Ag-HA samples. This can be attributed due to the proper substitution of Ca with metal ion during the preparation process. It has been reported that Ca deficient apatite (Ca/P atomic ratios between 1.33-1.55) could be very beneficial to the formation of new bone *in vivo* [36]. Thus, Ag-doped HA could be beneficial for the formation of new bone *in vivo*. Atomic ratios suggest the obtained samples are stoichiometric.
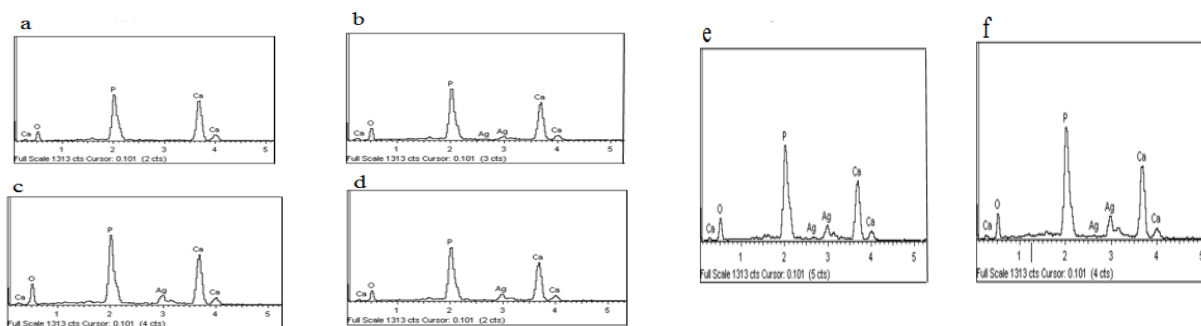

Figure 4: EDS spectrum of (a) pure HA, (b) Ag-HA-1, (c) Ag-HA-2, (d) Ag-HA-3, (e) Ag-HA-4, and (f) Ag-HA-5

TEM studies

Moreover, the size and shape of HA and Ag-HA were estimated from TEM analysis. Figure 5 shows TEM images of HA and Ag-HA-5. The HA nanoparticles were cylindrical rod-like shape with homogeneous microstructure, around 100 nm in diameter and several particles seem to aggregates. However, the particle sizes of Al-HA-5 about 100 nm and decreased significantly with the existence of Al element. The diameters of particles are slightly larger than the observed crystal sizes obtained from XRD, due to the presence of Nano crystalline surface layers as well as high temperature calcinations (950°C) which causes the grain growth. The selected area of electron diffraction patterns (SAED) of HA and Ag-HA5 shows in inset of Figures 6a and 6b. The bright ring patterns indicating the polycrystalline nature of nanoparticles.
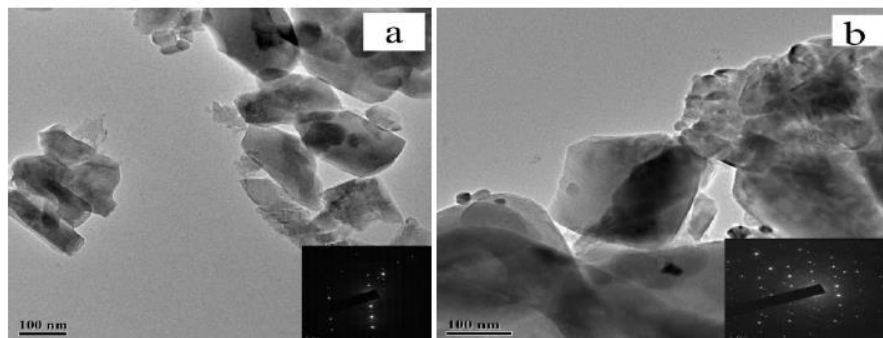

Figure 5: TEM images of (a) HA, (b) Ag-HA-5. (Inset: corresponding SAED pattern)

Antimicrobial activity evolution

To evaluate the Antibacterial effect, the bacteria were cultivated with various Nano crystals for a series of time and re-cultivated on agar according to the bacteria counting method. The percentage of Bacterial survival for *E. coli* and *S. aureus* as a function of time are shown in Figure 6. The bacteria reduction of Ag-HA nanocrystals exhibit dose-concentration and time-dependent features. The antibacterial rates of Ag-HA (0.05 ppm) are enhanced from 40% to 63% when the incubation time extended from 2.5 h to 15 h. Moreover, the antibacterial rate increases from 70% to 99% after 15 h incubation when the Ag doping concentration is enhanced from 0.05 ppm to 190 ppm. The effective antibacterial ability is defined as a percentage of bacteria reduction above 70% for *S. aureus* and *E. coli*.
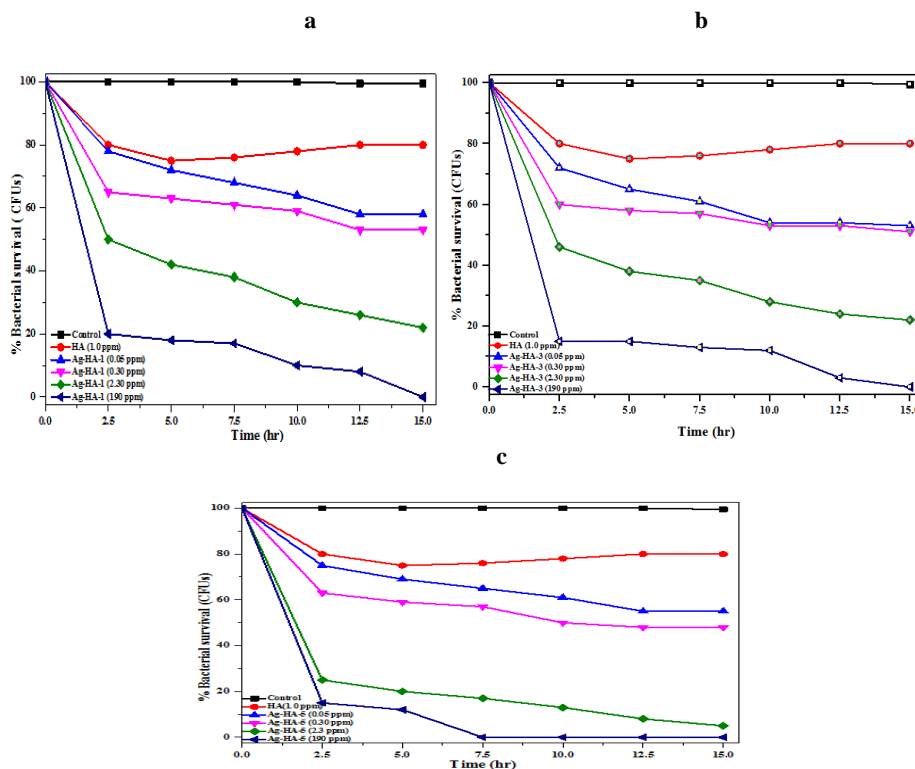

Figure 6a: Percentage of bacteria survival for *Escherichia coli* as a function of time for (a) Ag-HA-1, (b) Ag-HA-3, (c) (b) Ag-HA-5 *Staphylococcus aureus*

Antibacterial results shows that the antibacterial rates are 85% and 93% when 0.30 ppm and 2.3 ppm Ag-HA Nano crystals are come in contact with bacteria. The maximum Concentration that exhibits effective antibacterial 2.3 ppm. The effective antibacterial activity of ultra-trace Ag-HA reveals that high doping concentration of Ag-HA is not necessary to achieve effective antibacterial activity for HA, appropriate amount of ultra-trace silver doping can also be adopted as an ideal option.
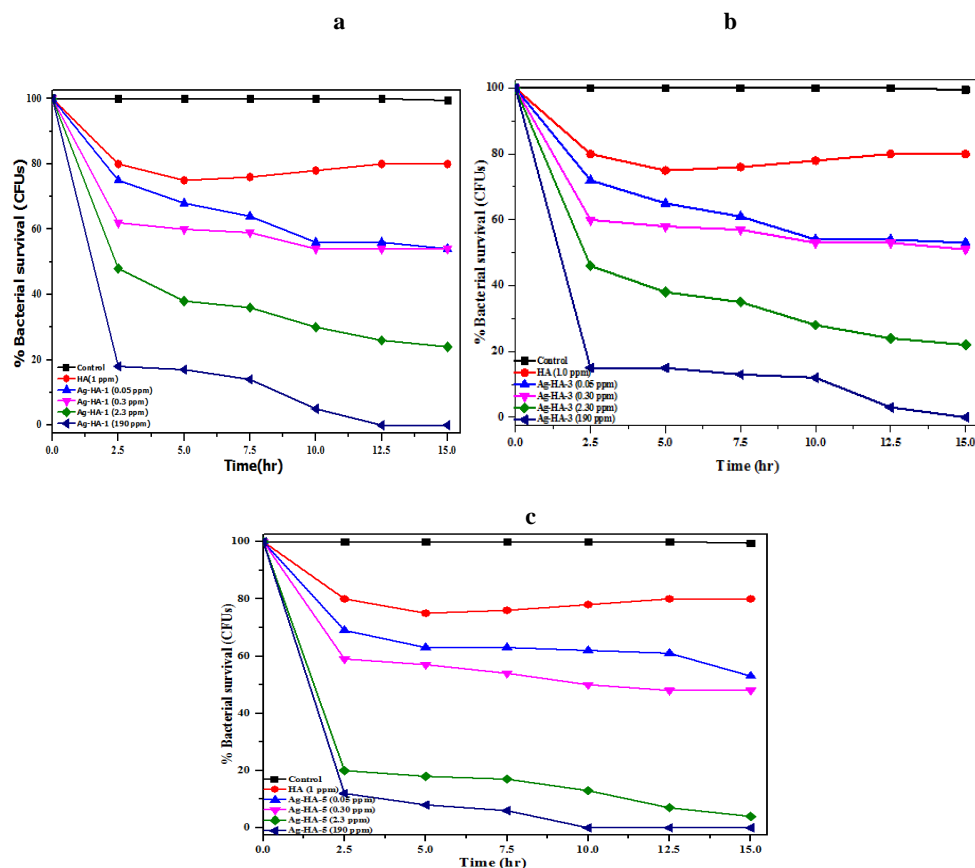

Figure 6b: Percentage of bacteria survival for *Staphylococcus aureus* as a function of time for (a) Ag-HA-1, (b) Ag-HA-3, (c) (b) Ag-HA-5

The physical and chemical characteristics such as morphology, chemical composition and surface properties of surrounding medium can be affect the viability of Bacteria [37]. Previous research have been revealed that antibacterial activity of Ag-HA, it is resulted from the release of Ag^+ [38]. The released of Ag^+ will bind to proteins on the membrane, thereby causing structural changes and damage to the membranes [39]. It was reported that release Ag^+ penetrates into cells and interacts with nucleic acids, preventing proliferation process and causing bacteria death [40].

In present research work Ag-HA (2.3 ppm) and Ag-HA (190 ppm), the bacteria were 90% and 99% reduced with the accumulated Ag^+release amount. However, the ultra-trace Ag-HA (0.30 ppm) also exhibited 82% bacteria reduction with Ag^+ release. It may be due to the contact antibacterial process that causes bacteria death at the surface of Ag-HA nanoparticles. When the bacteria contact Ag-HA nanoparticles, the bacteria were killed due to the high concentration of Ag^+at Ag-HA surface.

When the Ag concentration is 0.05 ppm accompanied by 63% antibacterial ratio upon further adding the doping concentration 2.3 ppm, the antibacterial activity was enhanced unceasingly to 83%. When Ag concentration comes to 190 ppm, 99% of bacteria were killed. The two curves come into an intersection between 0.30 ppm and 2.3 ppm Ag-HA, which exhibited 85% antibacterial activity. It has been reported that the antibacterial properties of Ag were dose-dependent [32,41-43]. Ag-HA-5 shows good antibacterial activity at low concentration and in appropriate time.

CONCLUSION

In present work The structural, composition and cytotoxic properties of the pure HA and Ag-HA nanoparticles with different stoichiometric ratios prepared by a modified solution combustion technique have been studied in great detail. The physicochemical properties of the pure HA have been affected with the existence of Silver. The pure HA and Ag-HA nanoparticles having pure phase and almost identical particle sizes. EDS analysis confirmed the presence of pure HA and Ag-HA with stoichiometric ratio and this material could be applicable for the formation of new bone *in vivo*. HA nanoparticles doped with Ag possess effective antibacterial activity and *in vitro* noncytotoxicity. The antibacterial rate increases from 65% to 99% while the cell viability decreases from 97% to 75% when the Ag-doping concentration varies from 0.05 to 190 ppm. The optimal properties with excellent cytocompatibility and antibacterial ability can be achieved when the Ag-doping concentration is between 0.30 ppm and 2.3 ppm. The antibacterial HA with Ag is non-toxicity to living cells and tissues even if the particles are internalized by cells. Hence, it is revealed that Taken together, Ag-HA nanocrystals are potentially applicable as bone substitution materials in tissue engineering. Ag-HA is an excellent candidate in the biomedical field.

REFERENCES

[1] A. Bigi, E. Boanini, K. Rubini, *J. Solid. State. Chem*., **2004**, 177, 3092-3098.

[2] L.L. Hench, J. Bioceramics, *Am. Ceram. Soc*., **1998**, 81, 1705-1728.

[3] K.D. Groot, C.P.A.T. Klein, J.G.C. Wolke, J.M.A. Blieck-Hogervorst, In: T. Yamamuro, L.L. Hench, J. Wilson, *CRC Press*, Boca Raton, FL, **1990**, P-3.

[4] R.Z. LeGeros, Osaka University, **2002**.

[5] M. Supovan, *Ceramics International.*, 41, **2015**, 9203-9231

[6] H.J. Qiu, J. Yang, P. Kodali, J. Koh, G.A. Ameer, *Biomaterials.*, **2006**, 27, 5845-5854.

[7] Y. Tanaka, Y. Hirata, R. Yoshinaka, *J. Ceram. Process. Res*., **2003**, 4 (4), 197-201.

[8] I. Smiciklas, A. Onjia, J. Markovic, S. Raicevic, *Mater. Sci. Forum*, **2005**, 494, 405-410.

[9] R.Z. LeGeros, *Chem. Rev*., **2008**, 108, 4742-4753.

[10] E.D.Berry, G.R. Siragusa, *Appl. Environ. Microbial*., **1997**, 63, 4069-4074.

[11] M. Niinomi, M. Nakai, J. Hieda, *Acta Biomaterialia*, **2012,** 8, 3888-3903.

[12] K.S. Oh, K.J. Kim, Y.K. Jeong, Y.H. Choa, *Key. Eng. Mater*., **2003**, 240-242, 583-586.

[13] M. Wakamura, K. Kandori, T. ishikawa, *Colloids Surface: A.*, **2000**, 164, 297.

[14] E.M. Hetrick, M.H. Schoenfisch, *Chem. Soc. Rev*., **2006**, 35, 780-789.

[15] U. Türkan, O. Öztürk, A.E. Eroğlu, *Orthopedic Implant Material.*, **2006**, 200, 5020-5027.

[16] N. Espallargas, C. Torres, A.I. Muñoz, *WEAR*., **2014**, 332-333.

[17] S.J. Lee J.J. Lai, *J Materials Processing Technol*., **2003**, 140, 206-210.

[18] C.C. Shih, C.M. Shih, Y.Y. Su, L.H.J. Su, M.S. Chang, S.J. Lin, **2004**, 46, 427-441.

[19] T.F. Zhang, Q.Y. Deng, B. Liu, B.J. Wu, F.J. Jing, Y.X. Leng, *CoCrMo and Ti6Al4V Substrate.,***2003**.

[20] B. Alemón, M. Flores, W. Ramírez, J. C. Huegel, E. Broitman, **2015**, 81, 159-168.

[21] V. Stanic, D. Janackovic, S. Dimitrijevic, S.B. Tanaskovic, M. Mitrica, M.S. Pavlovic, A. Krstic, D. Jovanovic, S. Raicevic, *Appl. Surf. Sci*., **2011**, 257, 4510-4518.

[22] J.R. Morones, J.L. Elechiguerra, A. Camacho, K. Holt, J.B. Kouri, J.T. Ramirez, M.J. Yacaman, *Nanotechnology*., **2005**, 2346-2353.

[24] C. Shi, J. Gao, M. Wang, J. Fu, D. Wang, Y. Zhu, *Mater. Sci. Eng. C*., **2015**, 55, 497-505.

[25] R. Murugan, S. Ramakrishna, *Acta. Biomater*., **2006**, 2, 201-206.

[26] M.H. Fathi, A. Hanifi, V. Mortazavi, *J. Mater. Process. Technol*., **2008**, 202, 536-542.

[27] G.C. Koumoulidis, A.P. Katsoulidis, A.K. Ladavos, P.J. Pomonis, C.C. Trapalis, A.T. Sdoukos, T.C. Vaimakis, *J. Colloid Interface. Sci*., **2003**, 259, 254-260.

[28] Z. Zou, K. Lin, L. Chen, J. Chang, *Ultrason. Sonochem*., **2012**, 19, 1174-1179.

[29] S. Lala, S. Brahmachari, P.K. Das, D. Das, T. Kar, S.K. Pradhan, *Mater. Sci. Eng*., **2014**, 42, 647-656.

[30] A.G. Merzhanov, *Bentham Sci*., **2012**, 112.

[31] S.T. Aruna, *Bentham Publishers.*, **2010**, 206-221.

[32] C. Shi, J. Gao, M. Wang, J. Fu, D. Wang, Y. Zhu, *Mat. Sci. Eng*., **2015**, C55, 497-505.

[33] N.D. Thorat, S.V Otari, R.M. Patil, V.M. Khot, A.I. Prasad, R.S. Ningthoujam, *Colloids. Surf. B. Biointerfaces*., **2013**, 111 264-269.

[34] F.A.C. Andradea, L.C.O. Vercikb, F.J. Monteiroc, E.C. Silva Rigoa, *Ceramics Int*., **2016**, 42, 2271-2280.

[35] M.J. Phillips, J.A. Darr, Z.B. Luklinska, I. Rehman, *Mater. Sci. Mater. Med*., **2003**, 14, 875-882.

[36] S.V. Dorozhkin, *Prog. Cryst. Growth Charact. Mater*., **2002**, 44, 45-61.

[37] S. Kang, M. Herzberg, D.F. Rodrigues, M. Elimelech, *Langmuir,* **2008**, 24, 6409-6413.

[38] Z.M. Xiu, Q.B. Zhang, H.L. Puppala, V.L. Colvin, P.J.J. Alvarez, *Nano Lett*., **2012**, 12, 4271-4275.

[39] W.K. Jung, H.C. Koo, K.W. Kim, S. Shin, S.H. Kim, Y.H. Park, *Appl. Environ. Microbiol*., **2008**, 74, 2171-2178.

[40] Q.L. Feng, J. Wu, G.Q. Chen, F.Z. Cui, T.N. Kim, J.O. Kim, *J. Biomed. Mater. Res*., **2000**, 52, 662-668.

[41] R.J. Chung, M.F. Hsieh, C.W. Huang, L.H. Perng, H.W. Wen, T.S. Chin, *J. Biomed. Mater. Res*., **2006**, 76B 169-178.

[42] T.V. Kolekar, N.D. Thorat, H.M. Yadav, V.T. Magalad, M.A. Shinde, S.S. Bandgar, J.H. Kim, G.L. Agawane, *Ceram. Int*., **2016**, 42, 5304-5311.

[43] A.E. Nel, L. Mädler, D. Velegol, T. Xia, E.M.V. Hoek, P. Somasundaran, *Nat. Mater*., **2009**, 8, 543-557.